Synthesis and stability of xenon oxides Xe_2O_5 and Xe_3O_2 under pressure

Agnès Dewaele[1], Nicholas Worth[2], Chris J. Pickard[3,4,5] , Richard J. Needs[2], Sakura Pascarelli[6], Olivier Mathon[6], Mohamed Mezouar[6] and Tetsuo Irifune[7,8]

[1]*CEA, DAM, DIF, F-91297 Arpajon, France*
[2]*TCM Group, Cavendish Laboratory, J J Thomson Avenue, University of Cambridge, CB3 0HE, United Kingdom*
[3]*Department of Physics and Astronomy, University College London, Gower Street, London WC1E 6BT, United Kingdom*
[4]*Department of Materials Science & Metallurgy, University of Cambridge, 27 Charles Babbage Road, Cambridge, CB3 0FS, United Kingdom*
[5]*Advanced Institute for Materials Research, Tohoku University 2-1-1 Katahira, Aoba, Sendai, 980-8577, Japan*
[6]*European Synchrotron Radiation Facility, BP220, 38043 Grenoble Cedex, France*
[7]*Ehime University, 2–5 Bunkyo-cho, Matsuyama 790-8577, Japan*
[8]*Earth-Life Science Institute, Tokyo Institute of Technology, Tokyo 152-8500, Japan*

The noble gases are the most inert atomic group, but their reactivity increases with pressure. Diamond-anvil-cell experiments and *ab initio* modelling have been used to investigate a possible direct reaction between xenon and oxygen at high pressures. We have synthesized two oxides below 100 GPa, Xe_2O_5 under oxygen-rich conditions, and Xe_3O_2 under oxygen-poor conditions. Xe_2O_5 has been observed using X-ray diffraction methods, its structure identified using *ab initio* random structure searching, and confirmed using X-ray absorption and Raman spectroscopies. The experiments confirm the recent prediction of Xe_3O_2 as a stable xenon oxide under high pressure. Xenon atoms adopt mixed oxidation states of 0 and +4 in Xe_3O_2 and +4 and +6 in Xe_2O_5. Xe_3O_2 and Xe_2O_5 form extended networks incorporating oxygen-sharing XeO_4 squares, while Xe_2O_5 additionally incorporates oxygen-sharing XeO_5 pyramids. Other xenon oxides (XeO_2, XeO_3) are expected to form at higher pressures. We find that xenon is more reactive under pressure than predicted previously.

The binding of the valence electrons to the ionic core of a noble gas atom decreases with atomic number, opening up the possibility of oxidation for the heaviest of them (Kr, Xe). Since the 1960s, compounds containing xenon in oxidation states of +2, +4, +6 and +8 have been synthesized[1], for instance molecular XeF_2[2,3], XeO_3 [4] and XeO_4 [5]. Recently, a new xenon oxide, XeO_2, was synthesized, in which Xe-O bonds form an extended network of XeO_4 squares connected by sharing oxygen atoms at their corners[6]. Under ambient conditions, xenon oxides are thermodynamically unstable and are synthesized using xenon fluorides as reactants. At moderate pressures, solid xenon forms weakly bonded compounds with other species, for instance with H_2O around 1 GPa[7] or O_2 around 3 GPa[8,9]. However, its properties change significantly when the pressure is further increased. Xenon transforms sluggishly between 3 and 80 GPa[10-12] from a face-centred cubic (fcc) to a hexagonal close packed (hcp) structure, which becomes metallic around 135 GPa[13].

Recently, theoretical proposals and experimental evidence have appeared for the formation of strongly bonded and stable xenon compounds under pressure. A recent theoretical study has proposed Xe-Ni and Xe-Fe structures, and found them to be stable against decomposition under conditions found in the Earth's inner core[14]. Xenon has been incorporated in quartz at pressures of a few GPa and high temperatures[15], and it has been proposed that xenon atoms replace silicon atoms in this structure. The synthesis of a compound of xenon, oxygen and hydrogen was reported recently at around 50 GPa[16]. The formation of xenon oxides in the Mbar range has been predicted using an evolutionary structure searching algorithm[17] and density functional theory (DFT) methods[18-20]. In Refs. 18 and 19, only the simple stoichiometries XeO, XeO_2, XeO_3 and XeO_4 suggested by low-pressure experimental observations were considered. Hermann and Schwerdtfeger found a Xe_3O_2 structure in searches and predicted it to be stable above 75 GPa[20]. However, experimental data for xenon oxides have not been reported previously at the high pressures at which they might become stable. Structure searching methods have been used in conjunction with first-principles DFT calculations to determine structures of boron[21], hydrogen[22] and many other materials at high pressures. Studies of xenon chemistry[14-16,18-20] have been performed in part to help in explaining the anomalously low xenon content of the Earth's atmosphere[23] in comparison with stony meteorites. One proposal for resolving this "missing xenon paradox" is that xenon is stored in the deep Earth, thus motivating a better understanding of the chemistry of xenon under geological pressures.

We have investigated the stability of compounds of xenon and the most abundant element in the Earth's mantle, oxygen, under pressure. Experimental results are reported from powder X-ray diffraction (PXRD), X-ray absorption (XAS), and Raman spectroscopy, in laser-heated diamond anvil cells loaded with Xe-O_2 mixtures (O_2 content varying between 11 mol.% and 64 mol.%, see Supplementary Table SI). We have used the *ab initio* random structure searching (AIRSS) approach[24,25] and DFT methods to predict low enthalpy structures at pressures of 83 GPa, 150 GPa and 200 GPa. An ensemble of random structures with reasonable volumes was generated, subject to constraints on the minimum initial distances

between atoms and on the symmetries of the structures. Each of these structures was relaxed to their local minimum in enthalpy; see the Methods for more information.

Combining experimental and theoretical approaches has enabled us to synthesize and identify two xenon oxide structures at high pressures: Xe_3O_2 (as predicted in Ref. 20) and the new Xe_2O_5.

Results

Oxygen-rich systems.

Above ~77 GPa, a reaction was observed under laser heating of Xe-O mixtures with an O_2 content higher than 50 mol.% that led to a single product (**1**), which was characterized by PXRD, XAS and Raman spectroscopies.

The PXRD pattern of product **1** recorded around 83 GPa (Fig. 1a) did not correspond to any of the xenon oxides that have previously been predicted[18-20]. This pattern was indexed by a tetragonal cell of volume $V = 247.3$ Å^3, and showed a minor amount of unreacted Xe. The PXRD intensities enabled the determination of the approximate atomic positions of the xenon atoms in the tetragonal cell, but not the precise number and positions of the oxygen atoms because of the low atomic scattering power of oxygen relative to xenon.

Characterization of **1** by XAS at the Xe K-edge showed the presence of Xe-O bonds. XAS near edge spectra of the sample compressed to 82 GPa are presented in Fig. 2a. Fig. 2b shows the extended X-ray absorption fine structure oscillations due to the local environment around the Xe atoms, and Fig. 2c shows their Fourier transform for the heated sample. A simple two shell model including only one Xe-O and one Xe-Xe coordination shell provides a good fit to the data, with 3.0±0.5 oxygen atoms and 5.0±0.6 xenon atoms at separations of 1.93 Å and 3.165 Å, respectively. We saw no evidence for contamination by unreacted xenon of the XAS spectra, and the absence of xenon was further confirmed by PXRD data taken on the same spot (see the Supplementary Information).

To identify the structure of xenon oxide **1**, we first used *ab initio* random structure searching (AIRSS) to determine the lowest-enthalpy structures of simple Xe-O stoichiometries — such as Xe, Xe_2O, XeO, XeO_2, XeO_3, and O — and their cell volumes at 83 GPa. We then added together simple stoichiometries, such as $XeO_2+2XeO=Xe_3O_4$. Multiplication by a suitable integer (e.g., $3Xe_3O_4$) then provided cell volumes that were compared with the experimental unit cell volume of **1**. A close match between theoretical and experimental cell volumes suggests a reasonable candidate structure, which is then checked against the available experimental data (PXRD, XAS and Raman spectroscopy). After several trials, we found that $4(XeO_2+XeO_3)=4Xe_2O_5$ provided a good match to the experimental unit cell volume of the xenon oxide. We then used AIRSS with the unit cell constrained to experiment to find the lowest-enthalpy structure of stoichiometry Xe_2O_5 with four formula units per cell. This procedure led us to a *P*4/*ncc* structure that, crucially, was found to have the lowest enthalpy with this stoichiometry (see Supplementary Fig. S2).

Simulated PXRD and XAS data for this theoretical Xe_2O_5 structure were in good agreement with the experimental data of **1** (see Figs. 1 and 2). The Raman spectrum of **1** was collected at 88 GPa (Fig. 3) and on subsequent pressure decrease (Supplementary Fig. S3). The Raman frequencies and intensities calculated at the same volume in Xe_2O_5 correctly reproduce this experimental spectrum, although all Raman frequencies are slightly lower (by ∼4 %) than in the experimental spectrum of product **1**, which suggests that the bond strength is underestimated in the calculations. The bulk modulus predicted by DFT calculations at this volume (313 GPa, in contrast to the experimentally measured value of 440 GPa, see Table I) further supports this interpretation, and the DFT and experimental data therefore provide strong evidence that the synthesized compound **1** is that of Xe_2O_5 adopting a *P*4/*ncc* structure.

The theoretical structure of Xe_2O_5 at 83 GPa is illustrated in Fig. 4a. It consists of a three-dimensional framework of corner-sharing XeO_4 squares with an Xe-O distance of 1.98 Å. Every second Xe atom bonds with a fifth O atom (Xe-O distance 1.83 Å), forming a XeO_5 square pyramid with the Xe atom being slightly below the base of the pyramid. These two similar Xe-O distances could not be resolved in the XAS data and appear as a single (average) Xe-O shell at 1.93Å. Such local geometries have been reported in molecules or solids containing oxidized xenon. This suggests the presence of Xe^{4+} and O^{2-} in XeO_4 units (as in XeO_2)[6] and Xe^{6+} and O^{2-} in XeO_5 units (as in $[XeF_5]^+[PtF_6]^-$)[26]. The minimum Xe-Xe distance is 3.19 Å, in agreement with the XAS data, and adjacent xenon atoms are connected by a single oxygen atom. Table I gives the lattice parameters and interatomic separations determined by experiment and DFT.

The experimental density of Xe_2O_5 is 14% higher than that of a mixture of xenon[8] and O_2[27] with the same stoichiometry and under the same pressure . Xe_2O_5 thus allows an efficient packing of xenon and oxygen atoms. Oxidation states of the Xe atoms determined using Mulliken, Bader and Hirshfeld charge density analyses[28–30] are consistent and confirm the oxidation states of +4 or +6 for Xe atoms in Fig. 4a (see Supplementary Table SIII). Xe atoms connected to each other via an oxygen atom have different oxidation states. The shortest distance between a Xe^{6+} ion and the four nearest oxygen atoms not bonded to it is only 2.29 Å (in contrast, for Xe^{4+} this distance is 2.49 Å). This small interatomic separation suggests a weak attraction between these atoms, as in $[XeF_5]^{+}[PtF_6]^{-}$ [26].

The Raman and PXRD data show that the Xe_2O_5 crystal **1** is metastable down to ≃30 GPa (see Supplementary Figs. S3 and S4), and becomes amorphous at lower pressures. However, the Xe-O bonding still remains after pressure release: a Raman mode with a frequency similar to metastable XeO_4[31] or XeO_3[32] was recorded at 0 GPa before the diamond anvil cell was opened (Supplementary Fig. S3). The equation of state of Xe_2O_5 synthesized at 93 GPa was measured under a pressure increase to 99 GPa and subsequent decrease to 30 GPa (Supplementary Fig. S4). It agrees well with the equation of state predicted by DFT, see Table I. Around 80 GPa, the bulk modulus (resistance to compression) of Xe_2O_5 is approximately 50% higher than that of pure xenon, indicating strong bonding.

Oxygen-poor systems.

Another xenon oxide, with a lower oxygen content than Xe_2O_5, was also predicted by AIRSS to be stable at high pressures: Xe_3O_2 with an orthorhombic *Immm* structure. These calculations support the prediction of this phase made independently in Ref. 20. In order to investigate the existence of this compound experimentally, Xe-rich Xe-O_2 mixtures were compressed and heated by laser. For mixtures with an O_2 content lower than 25 mol.% a compound **2** was obtained that was indeed shown by PXRD to be Xe_3O_2. Apart from one intense extraneous peak, the Raman spectrum collected for **2** is in agreement with the predicted one for Xe_3O_2, (Fig. 3), which coexists with both Xe and Xe_2O_5 — even for the mixture containing only 11% O_2 (Fig. 1), in contrast to the expected mixture of Xe_3O_2 and xenon. This may be due to the presence of an oxygen-rich $Xe(O_2)_2$ phase in the starting mixture (see Methods). The measured cell volume of Xe_3O_2 was 131.5 $Å^3$/2 formula units at 97 GPa, which is 8% denser than a mixture of xenon and O_2 at the same pressure.

The structure of Xe_3O_2 obtained with AIRSS is shown in Fig. 4b. Xe_3O_2 contains planar chains of XeO_4 squares parallel to the *b* axis, sharing oxygen corners as in the structure proposed for XeO_2[6]. This suggests a +4 oxidation state for these Xe atoms, bridged by four O^{2-} ions and forming a fully saturated network of XeO_2 stoichiometry. This is confirmed by charge density analysis (see Supplementary Table SIV). The layers of XeO_4 chains are intercalated with xenon layers, which are found to be unoxidized. As expected from the structure, the *b* axis parallel to the strong Xe-O chains undergoes less compression under pressure than the *a* and *c* axes (Supplementary Fig. S4). There is good agreement between the experimental and DFT values of the lattice parameters and interatomic distances of Xe_3O_2 at 97 GPa, which are summarized in Table I. The Xe^0–Xe^0 and Xe^0–Xe^{4+} distances are comparable to the Xe-Xe distance in pure xenon (3.03 Å)[8] at the same pressure. In Ref. 20, a small transfer of charge between Xe^0 and Xe^{4+} was calculated and interpreted as stabilizing this mixed valence compound, and our calculations support this analysis.

A Xe_2O oxide with a *C*2/*m* structure has been predicted by DFT searches[20] and confirmed by the current calculations to be stable at high pressure. Indeed, several xenon-rich structures predicted by DFT searches to be stable or close to stability, both previously[20] and in this study, are closely related to Xe_3O_2, but with larger fractions of intercalated Xe atoms, see Fig. S2. In the present experiments, we did not observe any evidence from PXRD for the synthesis of the Xe_2O-*C*2/*m* phase.

Xe_3O_2 was found to be metastable down to ~38 GPa before amorphisation. Our DFT calculations predict that Xe_2O-*C2/m* is stable above 65 GPa, and Xe_3O_2 above 66 GPa. The equation of state of Xe_3O_2 measured on pressure decrease is in good agreement with DFT close to the synthesis pressure (see Supplementary Fig. S4). The measured bulk moduli of Xe_3O_2, in which 2/3 of the xenon atoms are unoxidized, and pure Xe are similar at high pressures. The bulk modulus of Xe_2O_5 at 97 GPa is about double that of Xe_3O_2 at 83GPa, which is compatible with stronger inter-atomic bonding in Xe_2O_5.

Discussion

Enthalpies of formation per atom of the most stable structures found in the searches are plotted against the fraction *x* of O atoms on a convex hull diagram in Fig. 5. Structures on the hull indicated by filled circles are stable. Xe_3O_2, Xe_2O_5 and Xe_2O were found to be stable compounds at around 1 Mbar. The substantial differences between the hull plots in Fig. 5 and those of Refs. 19 and 20, which are directly compared in Supplementary Fig. S1, arise from two main sources.

(1) We have searched over 17 stoichiometries (not including pure Xe and O, see Supplementary Fig. S2) to identify possible stable structures with up to 28 atoms in the primitive unit cell, which involved relaxing about 10^5 structures. Zhu *et al.*[19] considered 4 stoichiometries (XeO, XeO_2, XeO_3 and XeO_4), but for each of their predicted structures we found either a lower-enthalpy structure or that the structure was unstable to decomposition into compounds on the convex hull with other stoichiometries. The searches in Ref. 20 were conducted over 8 stoichiometries, which included Xe_3O_2, which they correctly found to be stable, although they did not consider Xe_2O_5.

(2) In Refs. 19 and 20 a pseudopotential was used to describe the Xe 4*d* orbitals. However, this approximation is inaccurate for xenon oxides and pure Xe at high pressures because of the spatial overlap of the Xe 4*d* orbitals and the higher energy 5*s* and 5*p* Xe orbitals, see Supplementary Figs. S5 and S6. For example, calculations for Xe_2O_5 give an enthalpy of formation from the elemental solids at 83 GPa of -0.37 eV per atom, but only -0.05 eV when the 4*d* orbitals are described by the pseudopotential, see Supplementary Fig. S7.

The densities of electronic states show substantial transfer of charge from Xe to O atoms in Xe_2O_5, which suggests strong ionic Xe-O bonding, see Supplementary Figs. S11 and S13. The transfer of charge from Xe to O in Xe_3O_2 is quite small, which is consistent with the observation that 2/3 of the Xe atoms are in the zero oxidation state.

The electronic band structure of Xe_2O_5 at 83 GPa is shown in Fig. 6. Band structures and densities of states of the other structures predicted to be stable in some pressure range are provided in Supplementary Figs. S12, S14 and S15. The occupied valence bands of Xe_2O_5 are divided into an upper part arising from the oxygen 2*p* and xenon 5*p* levels with a width of approximately 12 eV, and a lower part from the oxygen 2*s* and xenon 5*s* levels with a width of approximately 15 eV. The Xe 4*d* bands are almost dispersionless and lie at about 60 eV below the highest occupied orbitals, and are not directly involved in chemical bonding.

Using the Perdew–Burke–Ernzerhof (PBE) semi-local density functional[33], Xe_2O_5 was predicted to be an insulator with a band gap of 1.48 eV at 83 GPa, while Xe_3O_2 was predicted to be semi-metallic with a very low density of states at the Fermi energy (see Supplementary Fig. S12). We also calculated the band gap of Xe_3O_2 using the HSE06 screened Coulomb functional[34], which normally gives larger and more accurate band gaps than PBE. A minimum band gap of about 0.05 eV was found with the HSE06 functional, which is close to the value

reported in Ref. 20 and suggests that Xe_3O_2 is a small band gap semiconductor at 83 GPa. Table II provides more information on the calculated band gaps of these xenon oxides.

DFT calculations were performed at higher pressures to investigate the evolution of the convex hull with compression (see Supplementary Table SII). We found the previously unreported phases XeO_3-$P2_12_12_1$ and XeO_2-*Pnma,* which become stable above around 131 GPa and 186 GPa, respectively. At about 191 GPa, Xe_2O becomes unstable to decomposition into Xe_3O_2 and Xe; around 197 GPa, Xe_2O_5 is predicted to decompose into a mixture of XeO_2 and XeO_3. These phases are depicted in Supplementary Figs. S8 and S9. The structural parameters of these phases are provided in Supplementary Table SV and bandstructures are given in Supplementary Table SVI and Supplementary Figs. S14 and S15. XeO_3 is an extended structure with all Xe atoms in a +6 oxidation state. XeO_2 consists of distorted versions of the XeO_2 chains found in Xe_3O_2. Both of these structures are more compact than Xe_2O_5, contributing to their greater stability at higher pressures.

The need for laser heating to induce chemical reactions in Xe-O_2 mixtures and the observation that Xe_2O_5 (Xe_3O_2) is metastable down to ~30 GPa (~38 GPa) implies the existence of substantial kinetic barriers between phases. The stability of the xenon oxides is found to increase substantially with pressure, see Fig. 5. The relative stabilities of phases are not expected to be altered significantly by heating to 3000 K[19].

In summary, we have synthesized two oxides, Xe_3O_2 and Xe_2O_5, in laser-heated diamond anvil cells. *Ab initio* calculations coupled with AIRSS have successfully predicted their structures and stability. These compounds are predicted to be stable above about 50 GPa, which is considerably lower than previous estimates[19,20] and indicates greater chemical reactivity in xenon oxides than previously thought. This is due to a more accurate treatment of xenon's 4*d* orbitals that is required under high compression. It is interesting to note that xenon atoms adopt mixed valence states in the oxides stable at the lowest pressure, yielding unusual stoichiometries. This may be a general trend in compounds formed under high compression.

Methods

Experimental procedures. Membrane diamond anvil cells were loaded at room temperature with xenon-oxygen mixtures (with a composition determined using O_2[35] and Xe[36] equations of state) in a high-pressure vessel. The mixtures were homogenized in the vessel over ~12 hours before loading. After loading, the pressure was increased to ~10 GPa and the sample was characterized with Raman spectroscopy. The crystallization of Xe-O_2 mixtures under pressure leads to three different solid phases (Xe with O_2 impurities, $Xe(O_2)_2$[9] and pure O_2). The diamond anvil cell was heated at 420 K for several hours to reduce compositional heterogeneities in the sample chamber. The pressure was then increased to the required value, and the sample was laser-heated for a few minutes at the centre of the sample chamber, on one or both sides. The temperature was estimated to be above 2000 K. The sample was characterized before and after heating with X-ray diffraction (PXRD), X-ray absorption spectroscopy (XAS) and/or Raman spectroscopy (see Supplementary Table SI). The reacted

zone was detected by mapping PXRD or XAS spectra (see Supplementary Fig. S16). In one run, the rhenium gasket was isolated from the sample chamber by a gold ring in order to verify that rhenium did not participate in the chemical reactions.

PXRD experiments were performed on the ID27 beamline of the European synchrotron Radiation Facility, ESRF. The angular dispersive (λ=0.3738 Å) XRD patterns were collected on a MARE345 or a MAR-CCD detector, located at a distance of ~300 mm from the sample. The X-ray beam was focused by two Kirkpatrick-Baez mirrors and cleaned by two pinholes to a 2×2.7 μm^2 full width at half maximum (FWHM) spot on the sample. PXRD spectra were treated using the Fit2d software[37] and the crystal structure and Xe positions in Xe_2O_5 were determined using Dicvol[38] and Fox[39] software. XAS experiments were performed on the BM23 beamline of the ESRF[40], at the K-edge of xenon (34.561 keV) calibrated using gaseous xenon. The beam was focused to 4×4 μm^2 FWHM using a pair of Kirkpatrick-Baez mirrors. We used nano-polycrystalline diamond anvils[41], which do not create any XAS parasitic signal due to Bragg diffraction. A high quality spectrum was recorded in a wide range in the reciprocal space (k_{max} = 18 $Å^{-1}$) which enabled a detailed quantitative analysis of the near-neighbour shells of Xe in the direct space. The XAS spectra were analysed with the Athena and Artemis softwares[42] to determine the local structure around xenon atoms. PXRD was also performed on BM23. On ID27 and BM23, the pressure was measured using the PXRD signal from unreacted xenon or a gold pressure marker placed at the edge of the sample chamber and their ambient temperature equations of state[8,43] were checked with the rhenium gasket PXRD signal and equation of state[44]. For the Raman measurements, the pressure was obtained using the high-frequency Raman edge of the diamond anvil[45].

***Ab initio* calculations.** We used the CASTEP planewave DFT code[46] with ultrasoft pseudopotentials[47] ($4d^{10}$ $5s^2$ $5p^6$ and $2s^2$ $2p^6$ electrons treated as valence for Xe and O, respectively), for all except the Raman intensity calculations for Xe_2O_5 and the HSE06 calculations, for which norm-conserving pseudopotentials (with Xe $5s^2$ $5p^6$ and O $2s^2$ $2p^6$ electrons treated as valence) were used. A plane-wave basis set energy cutoff of 400 eV was used for the structure searches, and a cutoff of 700 eV was used for the final converged results reported in our paper. We employed the Perdew-Burke-Ernzerhof (PBE) generalized gradient approximation (GGA) density functional[33] for the calculations, except for the calculation of the band gap of Xe_3O_2 with the HSE06 functional[34]. The Brillouin zone was sampled using a k-point grid of spacing 2π×0.07 $Å^{-1}$ for the structure searches, and a finer spacing of 2π×0.03 $Å^{-1}$ for the final converged results.

We used AIRSS[24,25] to search for low-enthalpy structures over a wide range of stoichiometries. Within the basic AIRSS approach a cell volume and shape is selected at random within a reasonable range, atoms are added at random positions to provide the desired stoichiometry, and the system is relaxed until the forces on the atoms are negligible and the pressure takes the required value. Repeating this procedure provides a relatively sparse sampling of the "structure space". We constrained the minimum separations between atomic pairs (Xe–Xe, Xe–O, O–O) in the initial structures, which helps to space out the atoms appropriately, while retaining a high degree of randomness. We performed searches with various different symmetry constraints, which is useful because low energy structures often possess

symmetries[48]. In this way sampling is focused on the regions of the "structure space" in which chemical intuition suggests that the lowest-enthalpy structures are likely to be found.

Images of structures were generated using VESTA[49]. PXRD patterns were calculated using PowderCell[50]. Densities of electronic states were calculated using OptaDOS[51].

Acknowledgements. The authors acknowledge the European Synchrotron Radiation Facility for provision of beamtime under proposals HS-4067 and HC-767. Financial support was provided by the Engineering and Physical Sciences Research Council (EPSRC) of the UK [EP/J017639/1]. Computational resources were provided by the High Performance Computing Service at the University of Cambridge and the Archer facility of the UK's national high-performance computing service, for which access was obtained via the UKCP consortium [EP/K014560/1]. C.J.P. is supported by the Royal Society through a Royal Society Wolfson Research Merit Award. Nano-polycrystalline diamond anvils were prepared based on JSPS grants (No. 25220712 and No.15H05829) to T.I. We thank M. Hanfland for use of his laser heating setup, and Paul Loubeyre, Stéphane Mazevet, Chrystèle Sanloup, and John Trail for helpful discussions.

Author contributions. A.D. proposed the research; A.D. and R.J.N. coordinated the research. A.D. performed the experiments with the help of O.M. and M.M. at the synchrotron source. T.I. provided the nanopolycrystalline diamond anvils. A.D. and S.P. analysed experimental data. N.W. and C.J.P. performed the theoretical and computational work. R.J.N., A.D. and N.W. wrote the paper. All authors commented on the manuscript.

[1] Grochala, W. Atypical compounds of gases, which have been called 'noble'. *Chem. Soc. Rev.* **36**, 1632–1655 (2007).

[2] Claassen, H. H., Selig, H. & Malm, J. G. Xenon tetrafluoride. *J. Amer. Chem. Soc.* **84**, 3593 (1962).

[3] Chernick, C. L. *et al.* Fluorine compounds of xenon and radon. *Science* **138**, 136 (1962).

[4] Smith, D. F. Xenon trioxide. *J. Am. Chem. Soc.* **85**, 816 (1963).

[5] Selig, H., Claassen, H. H., Chernick, C. L., Malm, J. G. & Huston, J. L. Xenon tetroxide: Preparation and some properties. *Science* **143**, 1322 (1964).

[6] Brock, D. S. & Schrobilgen, G. J. Synthesis of the missing oxide of xenon, XeO_2, and its implications for Earth's missing xenon. *J. Am. Chem. Soc.* **133**, 6265–6269 (2011).

[7] Sanloup, C., Mao, H.-K. & Hemley, R. J. High-pressure transformations in xenon hydrates. *Proc. Natl. Acad. Sci. USA* **99**, 25–28 (2002).

[8] Dewaele, A., Loubeyre, P., Dumas, P. & Mezouar, M. Oxygen impurities reduce the metallization pressure of xenon. *Phys. Rev. B* **86**, 014103–014107 (2012).

[9] Weck, G., Dewaele, A. & Loubeyre, P. Oxygen/noble gas binary phase diagrams at 296 K and high pressures. *Phys. Rev. B* **82**, 014112–014119 (2010).

[10] Jephcoat, A. *et al.* Pressure-induced structural phase transitions in solid xenon. *Phys. Rev. Lett.* **59**, 2670–2673 (1987).

[11] Cynn, H. *et al.* Martensitic fcc-to-hcp transformation observed in xenon at high pressure. *Phys. Rev. Lett.* **86**, 4552–4555 (2001).

[12] Caldwell, W. A. *et al.* Geochemistry of xenon at high pressures. *Science* **277**, 930–933 (1997).

[13] Goettel, K. A., Eggert, J. H., Silvera, I. F. & Moss, W. C. Optical evidence for the metallization of xenon at 132(5) GPa. *Phys. Rev. Lett.* **62**, 665–668 (1989).

[14] Zhu, L., Liu, H., Pickard, C. J., Zou, G. & Ma, Y. Reactions of xenon with iron and nickel are predicted in the Earth's inner core. *Nature Chem.* **6**, 644–648 (2014).

[15] Sanloup, C., Schmidt, B. C., Perez, E. M. C., Gregoryanz, E. & Mezouar, M. Retention of xenon in quartz and Earth's missing xenon. *Science* **310**, 1174–1177 (2005).

[16] Sanloup, C., Bonev, S. A., Hochlaf, M. & Maynard-Casely, H. E. Reactivity of xenon with ice at planetary conditions. *Phys. Rev. Lett.* **110**, 265501 (2013).

[17] Glass, C. W., Oganov, A. R. & Hansen, N. USPEX– evolutionary crystal structure prediction. *Comput. Phys. Comm.* **175**, 713 (2006).

[18] Jung, D. Y. Ab Initio Studies in High Pressure Geochemistry. *Ph.D. thesis*, ETH Zürich (2008).

[19] Zhu, Q. *et al.* Stability of xenon oxides at high pressures. *Nature Chem.* **5**, 61–65 (2013).

[20] Hermann, A. & Schwerdtfeger, P. Xenon suboxides stable under pressure. *J. Phys. Chem. Lett.* **5**, 4336 (2014).

[21] Oganov, A. R. *et al.* Ionic high-pressure form of elemental boron. *Nature* **457**, 863–867 (2009).

[22] Pickard, C. J. & Needs, R. J. Structure of phase III of solid hydrogen. *Nature Physics* **3**, 473–476 (2007).

[23] Shcheka, S. S. & Keppler, H. The origin of the terrestrial noble-gas signature. *Nature* **490**, 531–534 (2012).

[24] Pickard, C. J. & Needs, R. J. Ab initio random structure searching. *J. Phys.: Condens. Matter* **23**, 053201 (2011).

[25] Pickard, C. J. & Needs, R. J. High pressure phases of silane. *Phys. Rev. Lett.* **97**, 045504 (2006).

[26] Bartlett, N., Einstein, F., Stewart, D. F. & Trotter, J. Crystal structure of $[XeF_5]^+$ $[PtF_6]^-$. *J. Chem. Soc.* (A) **7**, 1190 (1967).

[27] Weck, G., Desgreniers, S., Loubeyre, P. & Mezouar, M. Single crystal structural characterization of the metallic phase of oxygen. *Phys. Rev. Lett.* **102**, 255503 (2009).

[28] Mulliken, R. S. Electronic population analysis on LCAO–MO molecular wave functions. I. *J. Chem. Phys.* **23**, 1833–1840 (1955).

[29] Bader, R. F. W. *Atoms in Molecules – A Quantum Theory* (Oxford University Press, New York, 1990).

[30] Hirshfeld, F. L. Bonded-atom fragments for describing molecular charge densities. *Theoret. Chim. Acta* **44**, 129–138 (1977).

[31] Huston, J. L. & Claassen, H. H. Raman spectra and force constants for OsO_4 and XeO_4. *J. Chem. Phys.* **52**, 5646–5648 (1970).

[32] Claassen, H. H. & Knapp, G. Raman spectrum of xenic acid. *J. Chem. Soc.* **86**, 2341 (1964).

[33] Perdew, J. P., Burke, K. & Ernzerhof, M. Generalized gradient approximation made simple. *Phys. Rev. Lett.* **477**, 3865 (1996).

[34] Heyd, J., Scuseria, G. E. & Ernzerhof, M. Hybrid functionals based on a screened Coulomb potential. *J. Chem. Phys.* **118**, 8207–8215 (2003).

[35] Stewart, R. B., Jacobsen, R. T. & Wagner, W. Thermodynamic properties of oxygen from the triple point to 300 K with pressures to 80 MPa. *J. Phys. Chem. Ref. Data* **20**, 917–1021 (1991).

[36] Sifner, O. & Klomfar, J. Thermodynamic properties of xenon from the triple point to 800 K with pressures up to 350 MPa. *J. Phys. Chem. Ref. Data* **23**, 63–152 (1994).

[37] Hammersley, A. FIT2D: An introduction and overview. Tech. Rep. ESRF97HA02, ESRF (1997).

[38] Boultif, A. & Louër, D. Indexing of powder diffraction patterns for low-symmetry lattices by the successive dichotomy method. *J. Appl. Cryst.* **24**, 987–993 (1991).

[39] Favre-Nicolin, V. & Cerny, R. A better FOX: Using flexible modelling and maximum likelihood to improve direct-space ab initio structure determination from powder diffraction. *Z. Kristallogr.* **219**, 847–856 (2004).

[40] Mathon, O. *et al.* The time-resolved and extreme conditions XAS (TEXAS) facility at the European Synchrotron Radiation Facility: the general-purpose EXAFS bending-magnet beamline BM23. *J. Synchrotron Rad.* **22**, 1548–1554 (2015).

[41] Ishimatsu, N. *et al.* Glitch-free X-ray absorption spectrum under high pressure obtained using nano-polycrystalline diamond anvils. *J. Synchrotron Rad.* **19**, 768–772 (2012).

[42] Ravel, B. & Newville, M. ATHENA, ARTEMIS, HEPHAESTUS: Data analysis for X-ray absorption spectroscopy using IFEFFIT. *J. Synchrotron Rad.* **12**, 537–541 (2005).

[43] Dewaele, A., Loubeyre, P. & Mezouar, M. Equations of state of six metals above 94 GPa. *Phys. Rev. B* **70**, 094112–094119 (2004).

[44] Anzellini, S., Dewaele, A., Occelli, F., Loubeyre, P. & Mezouar, M. Equation of state of rhenium and application for ultra high pressure calibration. *J. Appl. Phys.* **115**, 043511 (2014).

[45] Akahama, Y. & Kawamura, H. Pressure calibration of diamond anvil Raman gauge to 410 GPa. *J. Phys.: Conf. Series* **215**, 012195 (2010).

[46] Clark, S. J. *et al.* First principles methods using CASTEP. *Z. Kristallogr*. **220**, 567 (2005).

[47] Vanderbilt, D. Soft self-consistent pseudopotentials in a generalized eigenvalue formalism. *Phys. Rev. B* **41**, 7892 (1990).

[48] Pauling, L. The principles determining the structure of complex ionic crystals. *J. Am. Chem. Soc.* **51**, 1010–1026 (1929).

[49] Momma, K. & Izumi, F. VESTA 3 for three-dimensional visualization of crystal, volumetric and morphology data. *J. Appl. Crystallogr.* **44**, 1272–1276 (2011).

[50] Kraus, W. & Nolze, G. POWDER CELL - a program for the representation and manipulation of crystal structures and calculation of the resulting X-ray powder patterns. *J. Appl. Cryst.* **29**, 301 (1996).

[51] Morris, A. J., Nicholls, R. J., Pickard, C. J. & Yates, J. R. OptaDOS: A tool for obtaining density of states, core-level and optical spectra from electronic structure codes. *Comp. Phys. Comm.* **185**, 1477–1485 (2014).

[52] Vinet, P., Ferrante, J., Rose, J. & Smith, J. Compressibility of solids. *J. Geophys. Res* **92**, 9319–9325 (1987).

TABLE I: Comparison of experimental and theoretical properties of Xe_2O_5 and Xe_3O_2. Experimental lattice constants were obtained from the PXRD data. Experimental interatomic distances were obtained using the structures from AIRSS and the experimental lattice constants. Lattice parameters and bond lengths are given at 83 GPa for Xe_2O_5 and at 97 GPa for Xe_3O_2. V_0 and K_0 denote the zero-pressure volume and bulk modulus obtained with a Rydberg-Vinet[52] fit of *P–V* data plotted in Supplementary Fig. S4. The error bars correspond to a 95% confidence level.

Xe_2O_5	**Experiment**	**Theory**
Lattice parameter *a* (Å)	4.980	4.978
Lattice parameter *c* (Å)	9.970	9.951
Volume (Å^3/4 f.u.)	247.3	246.6
Bond Xe^{6+}-O(1) (Å)	1.83	1.83
Bond Xe^{6+}-O(2) (Å)	1.97	1.97
Bond Xe^{4+}-O (Å)	1.98	1.98
Bond Xe^{6+}- Xe^{4+}(Å)	3.19	3.19
Rydberg-Vinet V_0 (Å^3/4 f.u.)	337.2±6	332.8±2.4
Rydberg-Vinet K_0 (GPa)	150±20	161±6
Rydberg-Vinet K'_0	4 (fixed)	4 (fixed)
Xe_3O_2	**Experiment**	**Theory**
Lattice parameter *a* (Å)	8 .457	8.388
Lattice parameter *b* (Å)	3.166	3.195
Lattice parameter *c* (Å)	4.904	4.880
Volume (Å^3/2 f.u.)	131.3	130.8
Bond Xe^{4+}-O (Å)	1.99	2.01
Bond Xe^{4+}- Xe^{4+} (Å)	3.17	3.19
Bond Xe^0-Xe^0 (Å)	3.06	3.05
Bond Xe^{4+}- Xe^0 (Å)	2.96-3.01	2.95-3.00
Rydberg-Vinet V_0 (Å^3/2 f.u.)	262±15	217.8±2.4
Rydberg-Vinet K_0 (GPa)	37.2±8	74.5±4
Rydberg-Vinet K'_0	4 (fixed)	4 (fixed)

TABLE II: Minimum (thermal) and minimum direct (optical) band gaps in eV calculated with the PBE exchange-correlation functional[33].

(a) Minimum band gap				
Structure	Pressure (GPa)			
	83	100	150	200
Xe_2O_5-*P*4/*ncc*	1.48	1.38	1.04	0.77
Xe_3O_2-*Immm*	0.00	0.00	0.00	0.00
(b) Minimum direct band gap				
Structure	Pressure (GPa)			
	83	100	150	200
Xe_2O_5-*P*4/*ncc*	1.80	1.76	1.65	1.55
Xe_3O_2-*Immm*	0.01	0.02	0.07	0.02

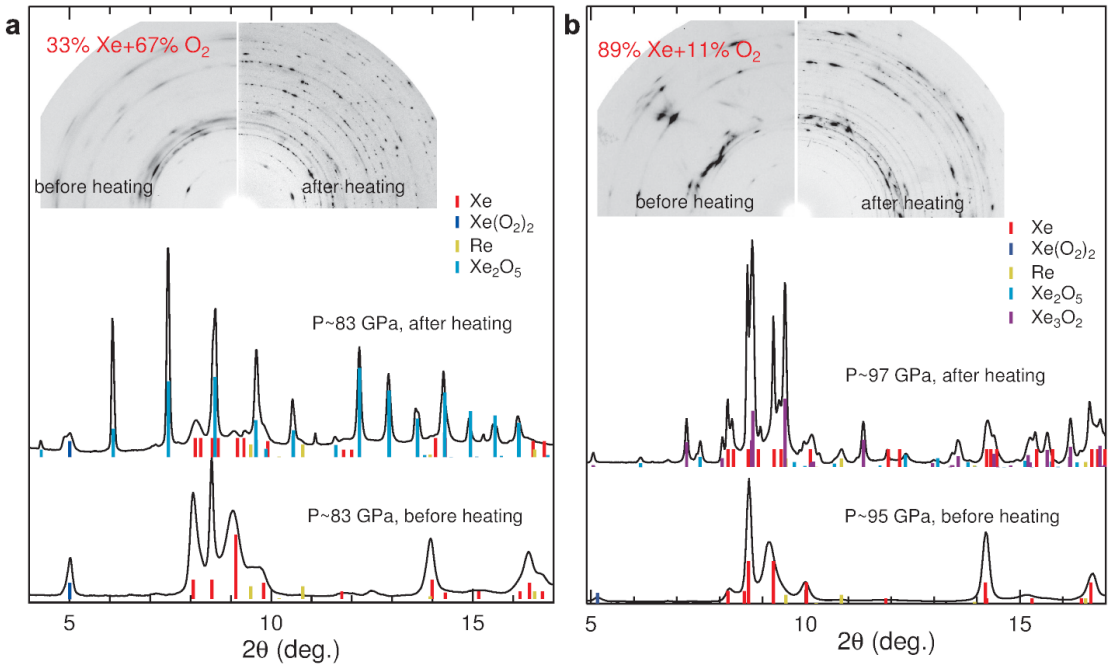

FIG. 1: X-ray diffraction patterns of Xe–O_2 mixtures under pressure. **a**, **b** X-ray diffraction patterns of a 33% Xe–67% O_2 mixture at about 83 GPa (a) and of a 89% Xe–11% O_2 mixture at about 97 GPa (b). The insets show the two-dimensional patterns before circular integration. Prior to laser-heating, the phases were Xe with O_2 impurities[8] and partially amorphized $Xe(O_2)_2$ [9] in both mixtures. After laser-heating, the phases consist of mostly Xe_2O_5 (a) and Xe_3O_2 and Xe_2O_5 (b), in addition to the reactants. The light blue and purple ticks indicate the positions and predicted relative intensities of the diffraction peaks of Xe_2O_5 and Xe_3O_2, respectively (lattice parameters in Table I). The most intense xenon diffraction peaks have been masked during integration. In both experiments, the Xe PXRD lines (red ticks) are split after laser-heating, which we interpret as arising from a variable content of O_2 impurities.

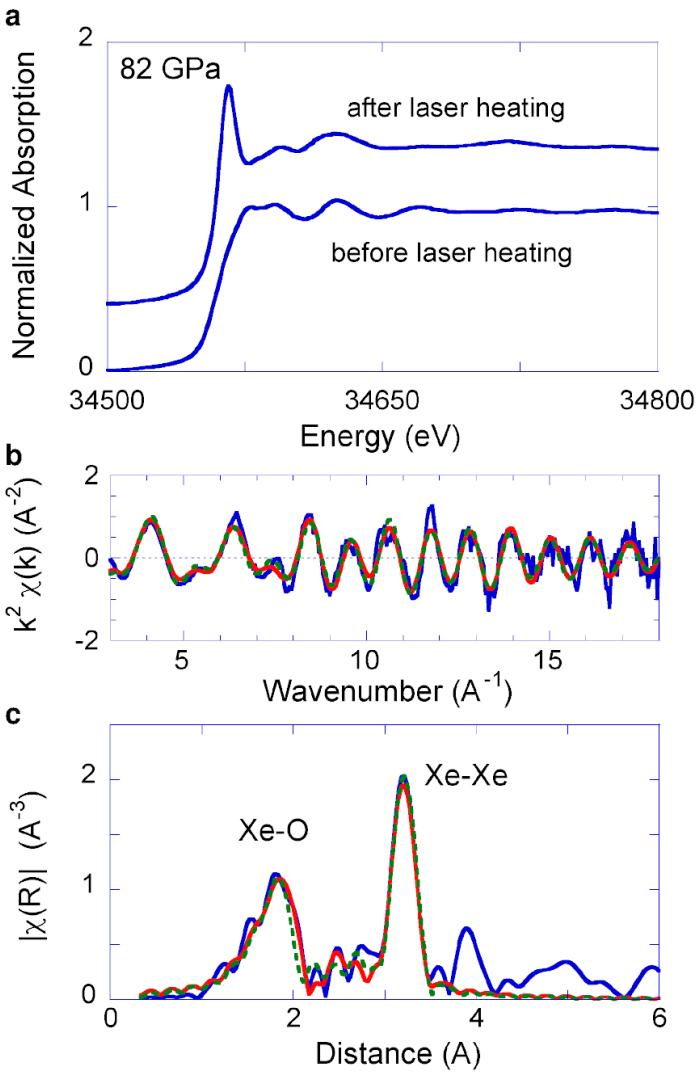

FIG. 2: Xe K-edge X-ray absorption spectra (XAS) of a 36% Xe – 64% O_2 mixture at about 82 GPa. a, Raw spectra. After heating, a strong absorption line appears at the Xe K-edge absorption onset (around 34.6 keV) at the centre of the laser-heated area, indicating depletion of the 5*p* states of Xe just above the Fermi level due to oxidation. **b**, Extended X-ray absorption fine structure function $\chi(k)$, weighted by k^2 (where k is the photoelectron wavenumber), extracted from the XAS spectrum after laser-heating (blue: data; dashed green: 2-shell fit; red: fit assuming the Xe_2O_5-*P4/ncc* structure). **c**, $|\chi(R)|$ (Å^{-3}) amplitude of the Fourier transform of this function (same colours as in **b**). The two intense peaks reflect the presence of two distinct distances with neighbours around xenon atoms. The abscissa has been rigidly shifted by 0.33 Å to account for the photoelectron scattering phase shift.

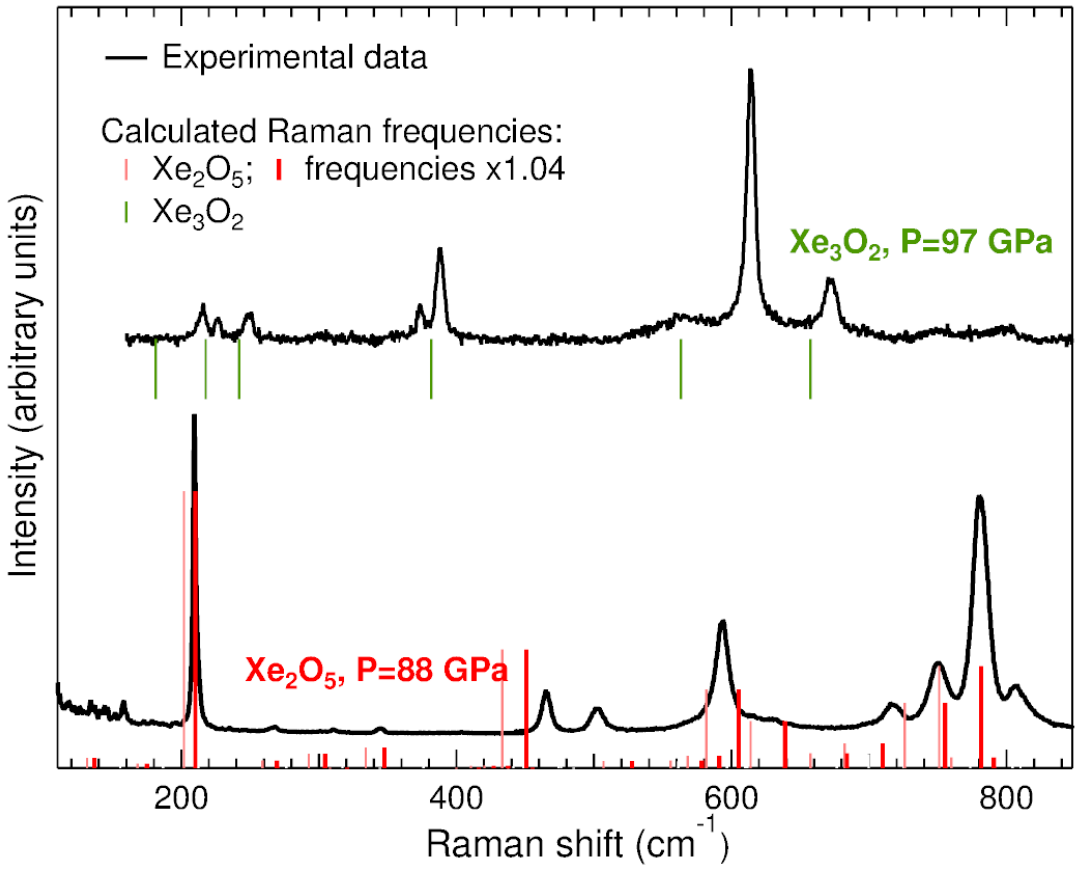

FIG. 3: Raman spectra of Xe_2O_5 and Xe_3O_2. Raman signals measured for Xe_2O_5 and Xe_3O_2 at 88 GPa and 97 GPa, respectively. Peak frequencies have been calculated for Xe_2O_5 and Xe_3O_2 at their experimental cell volumes and are plotted as red and green ticks, respectively. Peak intensities have also been calculated for Xe_2O_5. When the frequencies calculated for Xe_2O_5 are increased by 4% (bold red ticks), they agree with the measured ones to within ±15 cm^{-1}.

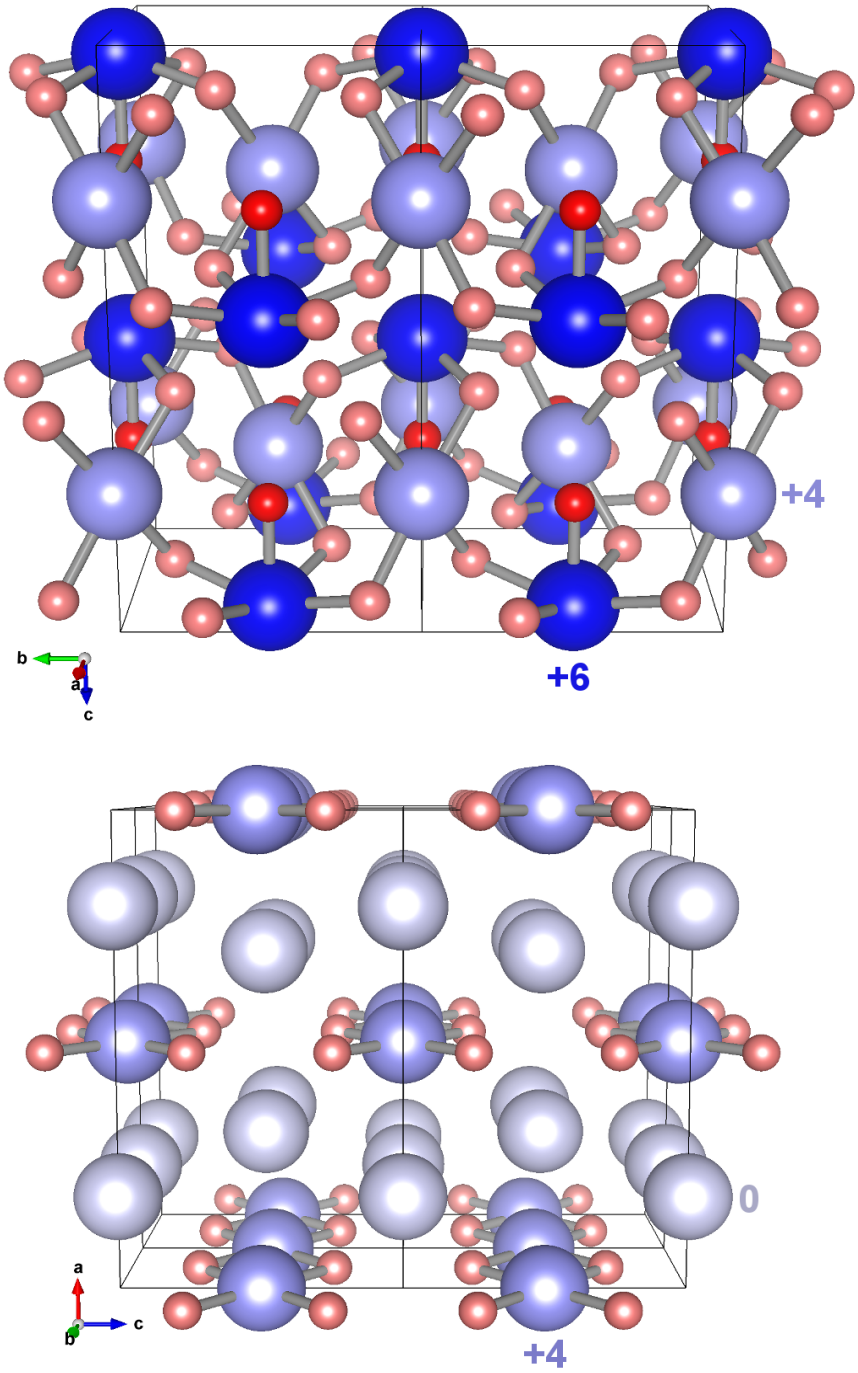

FIG. 4: Structures of the stable xenon oxides at 83 GPa. a, Xe_2O_5 and **b**, Xe_3O_2 . Xenon atoms are shown in blue shades and oxygen atoms in red shades. The oxygen atoms have an oxidation state of -2, and the darker shade of red indicates an oxygen atom that bonds only to one xenon atom. The oxidation states of the xenon atoms are indicated by different shades of blue. The lightest blue indicates 0 oxidation state, the medium shade +4 and the darkest blue the +6 oxidation state. The xenon atoms in Xe_2O_5 and Xe_3O_2 exist in two different oxidation states within each structure, +4 and +6 in Xe_2O_5 and 0 and +4 in Xe_3O_2.

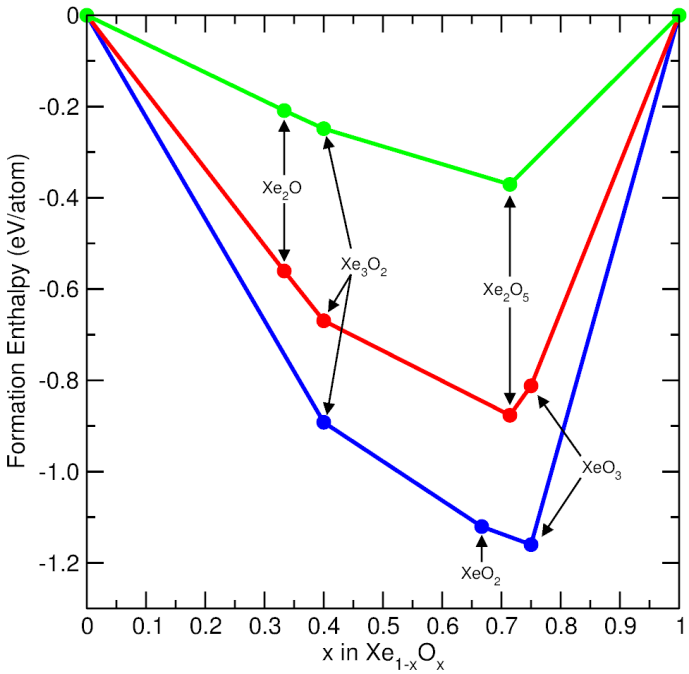

FIG. 5: Convex hull diagram for xenon oxides showing calculated enthalpies of formation per atom from the elements for the predicted stable phases. For a structure of stoichiometry Xe_mO_n, the enthalpy of formation per atom is given by $\Delta H_f(Xe_mO_n)=[H(Xe_mO_n) - (mH(Xe) + nH(O))]/(m+n)$, where H denotes the enthalpy of each formula unit under the relevant pressure. The three convex hulls shown are for 83 GPa (green), 150 GPa (red), and 200 GPa (blue). Each coloured circle denotes a structure that is stable against decomposition. The coloured lines joining the enthalpies of the stable structures denote the convex hull.

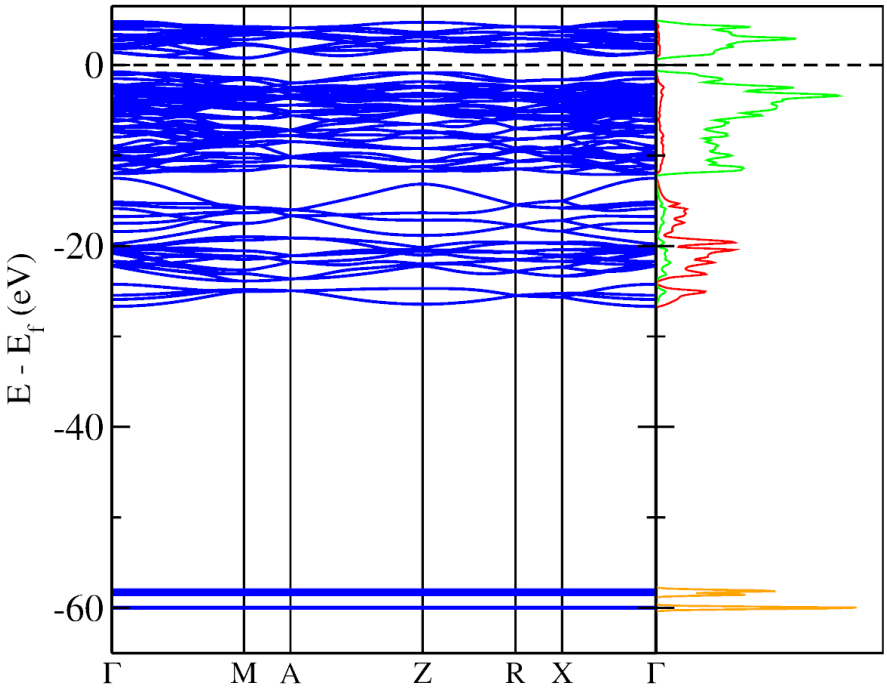

FIG. 6: Bandstructure and electronic density of states of Xe_2O_5 at 83 GPa. The electronic bands are shown in blue and the Fermi level is shown as a horizontal black dashed line. The orange line shows the *d* electron density of states (rescaled to fit on the axes), the red shows the *s* density of states, and the green shows the *p* density of states. Note the appearance of a band gap and that the *d* levels are about 30 eV below the *s* bands.